PAPER REF: 3828

AUTOMATIC SEGMENTATION ALGORITHM FOR THE LUMEN OF THE CAROTID ARTERY IN ULTRASOUND B-MODE IMAGES

André M.F. Santos[1(*)], João M. R.S. Tavares[1], Luísa Sousa[1], Rosa Santos[2], Pedro Castro[2], Elsa Azevedo[2]

[1] Faculdade de Engenharia, Universidade do Porto, Portugal

[2] Faculdade de Medicina, Universidade do Porto, Portugal

[(*)] *Email:* andremfs52@fe.up.pt

ABSTRACT

A new algorithm is proposed for the identification and segmentation of the lumen and bifurcation boundaries of the carotid artery in 2D longitudinal ultrasound B-mode images. It uses the hipoechogenic characteristics defining the lumen of the carotid for its identification and echogenic characteristics for the identification of the bifurcation. The input image is preprocessed with the application of an anisotropic diffusion filter for speckle removal, and morphologic operators for the detection of the artery. This information is then used for the definition of two initial contours, one corresponding to the lumen and the other to the bifurcation boundaries, for the posterior application of the Chan-Vese level set model.

A set of longitudinal B-mode images of the CCA was acquired, using a GE Healthcare Vivid-e ultrasound system, with 256 gray levels. All these images include a part of the CCA and the bifurcation that separates the CCA into the ICA and ECA. In order to achieve robustness in our acquisitions, with the highest contrast and lowest speckle noise levels as possible, the parameter settings of the scanner were different for each acquisition according to the associated image characteristics.

We were able to successfully apply a carotid segmentation technique based on cervical ultrasonography. The main advantage of our segmentation method relied on the automatic identification of the carotid lumen, overcoming the limitations of traditional methods.

Keywords: Medical Imaging; Image Analysis; Image segmentation; Deformable Models; Chan-Vese Model; Carotid Artery

INTRODUCTION

The common carotid artery (CCA) is the one supplying the human head, specifically the front part of the brain, and neck, with oxygenated blood. It is known for its paired structure, one for each half of the human body. The left common carotid artery has its origin in the aortic arch, while the right common carotid originates in the neck, specifically in the brachiocephalic trunk and containing a small thoracic portion. The CCA divides in the neck, where its bifurcation is situated, originating the internal and the external common carotid arteries: ECA and ICA, respectively. The ICA is characterized by its low resistance waveforms and its lateral and posterior disposition, compared to the ECA. The ECA extends anteriorlly and medially to the ICA, supplying the face, scalp, neck and tongue with blood, being also characterized by its high resistance waveforms. Like other arteries, which purpose relies in the supply of blood to the heart (coronary arteries), the carotid is also in risk of developing several diseases, like atherosclerosis, known as the “hardening of the artery”.

Atherosclerosis is an inflammatory disease, dominant in the blood vessel, consequently after the accumulation of fatty substances (lipoproteins) and cholesterol in the artery walls. This accumulation is known as plaque and causes the narrowing (stenosis) of the artery, decreasing the blood supply. In the case of the carotid artery, the bifurcation (separating the external and internal carotid arteries) and the internal carotid artery (ICA) are the structures more susceptible to atherosclerosis, due to the greater hemodynamic forces found at the bifurcation and branching structures.

Non-invasive ultrasound imaging is widely used in the diagnosis of cardiovascular diseases, like atherosclerosis, with the evaluation of the intima-media thickness (IMT), measuring the distance between the lumen of the carotid artery (where the blood flows) and the inner boundary of the adventitia. This measure, and consequent diagnosis of atherosclerosis, between other cardiovascular diseases, is performed with the aid of B-mode ultrasound imaging, requiring the detection of not only the lumen boundaries, as well as both the near and far adventitia. Therefore, it has been and continues to be a great interest in the performance of an automatic segmentation of the adventitia and lumen boundaries in B-mode ultrasound images of the carotid artery. According to Halenka (1999), in this type of images, the carotid adventitia is illustrated as two almost parallel lines, known for their echogenic characteristics, separated in the middle by a hipoechogenic space, known as the “double line” pattern (Halenka, 1999).

Ultrasound B-mode imaging is the most widely used technique in this type of medical image acquisition due to the fact of the carotid being a superficial artery and quite suitable for this type of imaging. However, B-mode images present difficulties, specifically in the segmentation step, due to several imaging characteristics, like low contrast and speckle noise, echo shadows and artifacts, having very poor quality and requiring the interaction of an active user. In ultrasound imaging, the speckle noise is presented in the form of granular texture in echogenic regions, where its intensity is related to the scanned tissue. Some works are found in the literature, where it is used several statistical distributions, like, for example, the Rayleigh distribution (Wagner et al., 1983; Sarti et al., 2004) and K-distribution (V. Dutt et al., 1994; R.C. Molthen et al., 1993), in order to deal and attenuate this granular speckle noise, being only applied to non-compressed signals. However, most of the signals that are actually used in ultrasound imaging and medical practice are known as log-compressed signals, which are unsuitable for the application of the distributions previously mentioned due to the reduced intensity range, characteristic of this type of signals. In 2006, Noble (Noble et al., 2006) described the success of texture segmentation techniques in the classification of breast masses and liver and kidney tissues specifically, in ultrasound images. However, in our specific case, regarding the classification of the carotid artery, it tends to be more difficult due to the extremely low degree of discrimination in ultrasound carotid images.

Ultrasound imaging represents an extreme and complex challenge in the performance of an automatic segmentation, as for the reasons described earlier, as for the amount of edges that may be missing in the image, producing gaps in vessel boundaries. Also, in the case of the carotid anatomy, in an ultrasound B-mode acquisition, scans may correspond to different portions of the carotid, illustrating distinguished structures of its anatomy and due to the variability of its shape between subjects; a model-based segmentation procedure is not robust enough for this type of segmentation. Despite these difficulties, there has been a great increase in the interest in ultrasound imaging medical diagnosis, as consequence of the technological advances verified in this methodology, not only in its quality, but also because of its non-invasive characteristics and cheaper cost (Rui Rocha et al, 2011).

The segmentation procedure can be considered as the logical sequence of two steps: (i) the definition or estimation of a region of interest (ROI) of the carotid artery in the B-mode ultrasound image and (ii) the delineation of the wall boundaries, depending on the ROI definition, as the wall (being lumen, or intima, or adventitia) which is to target. For this reason, we may consider that these two steps are not independent from each other, since the correct delineation of the artery wall in the segmentation algorithm is strictly connected to the correct definition of the ROI.

Between 1992 and 1994, occurred the first approaches for the identification and consequent segmentation of the carotid boundaries in B-mode ultrasound images, with the works developed by Touboul (1992), Gariepy (1993) and Selzer (1994) (Touboul et al., 1992; Gariepy et al., 1993; Selzer et al., 1994). At this time, the computing and segmentation techniques were not as advanced as nowadays, reason why all these works include a previous manual segmentation of the boundary of the carotid in order to proceed with its detection. This detection was performed according to only one local image feature, like the echo or the gradient intensities. Despite their importance, for they were the first attempts to detect the carotid artery, all these segmentation approaches suffer from some disadvantages: first, due to the enormous amount of time required for each one of these approaches, mainly due to the manual segmentations taken in each one of them; second, the identification of the carotid boundaries cannot be correctly performed based in a single image feature, since it can be affected to speckle noise, low contrast and possible discontinuities in the carotid boundaries.

In 1996, Kozich proposed a more robust approach, based on the minimization of a cost function by dynamic programming. Unlike Touboul (1992), Gariepy (1993) and Selzer (1994), Kozich (1996) integrated multiple image features for the development of his cost function. Not only had he considered the echo intensity and its gradient, like the previous works, but also a local constraint in order to originate a smoothed contour of the carotid boundaries. Each feature or constraint considered in Kozich’s work is represented by a cost term, usually a constant, representing the importance, or in other words, the weight of each feature in the development of the contour. Because of these cost terms, this model produced a more robust segmentation, when comparing to the ones developed in previous studies, with much less human intervention and time consuming. However, kozich’s model is also related to certain disadvantages: for example, its performance is directly affected by the presence of plaques, and so it is unsuitable for the correct detection of the carotid boundaries in patients with atherosclerosis; also, with this type of models, there is frequently needed some human intervention for contour correction when the image quality is lower. It is also required an intense search, for the optimal values of each image feature or constraint, where they have to be searched differently for images acquired with distinct ultrasonic equipments in some cases.

More recent studies showed great improvements with these problems, with the development of a different type of algorithms, called deformable models. These models center in the optimization of a cost function, in the search of a compromise between some of the methodologies applied by Kozich (1996) and even by Touboul (1992), Gariepy (1993) and Selzer (1994), typically defining the smoothness and continuity of the contour through adjacent points of the model, with the incorporation of an external force, attracting the contour towards the closest image edge. Deformable models can be distinguished in two classes: Parametric models, comprising the active contours, also known as Snakes; and Geometrical models, usually known as Level Sets.

There are studies published in the literature, especially those developed by Cheng (1999 and 2002), Schmidt (2001) and Jiaoying (2011), Matsakou (2011), Izquierdo (2011), for the specific segmentation of the common carotid artery using active contours. However, it can be also found the application of this methodology in the segmentation of other structures in ultrasound imaging, like the bladder and liver, as well as in other imaging acquisitions, like MRI and CT. Despite this, parametric snakes may not be the best choice for the automatic and correct segmentation of the carotid artery wall. This happens because the parametric snakes propagation force is based on intensity gradients and so, they tend to become stuck in local regions with minimal solutions, usually between the snake active contour and the real boundary and characterized by speckle noise, false edges or wall gaps the intensity gradient is extremely low or even null. Also, parametric snakes normally require manual initialization, with the design of the initial contour in the close vicinity of the carotid boundaries, implying a constant human intervention.

On the other hand, geometrical models present several advantages when compared to parametric models. The simple generalization when they are converted from two spatial dimensions to three or even more, as well as their easy treatment on the image regions with topological changes in the propagating fronts, in cases where there is a join in the contours or even when they are pressed towards each other. There are also several works for the segmentation of the common carotid artery based on geometrical models, where it can be distinguished the studies performed by Petroudi (2011) and Cheng (2011). Petroudi et al (2011) developed an algorithm which uses parametrical snakes, combined with active contours without edges, also known as the Chan-Vese geometrical deformable model, in order to detect the intima-media boundary of the carotid. On the other hand, Cheng et al (2011) made a comparison between three different geometric models on the detection of atherosclerosis carotid plaques. Cheng (2011) tested the Geodesic Active Contour (GAC) Model, the Chan and Vese Model and the Localizing Region-Based Active Contour Model. It was concluded that, when the initial contour of the deformable model was close to the boundary of interest, the localizing region-based model was the most suitable for the detection of atherosclerosis carotid plaques from ultrasound images of the CCA. Both studies of Petroudi (2011) and Cheng (2011) proof that geometric models are capable of performing a reasonable detection of the carotid wall boundaries, not only in healthy patients, but also for patients with atherosclerotic carotid plaques, with the proper use of some of these models. The time required for this type of segmentation is also suitable, and significantly reduced compared to the one required by parametric snakes.

In this paper, a method is proposed for the automatic identification of the lumen region and consequent segmentation of the lumen boundaries in longitudinal B-mode images of the CCA. The proposed method search for hipoechogenic structures in the input image and through mean intensities and standard deviation calculations, the lumen region of the CCA is identified. Consequently, the lumen and bifurcation boundaries of the carotid artery are identified through the application of a geometrical model, in particular, the Chan-Vese level set model. The method is robust to speckle noise, with no human interaction and the segmentation can adjust the contour with great flexibility, according to the shape of the lumen boundaries.

METHODS

The approach developed is depicted in the block diagram shown in Figure 1. The result is an estimation of the lumen and bifurcation boundaries. The method starts by isolation the ultrasound image environment from the rest of the image features (like acquisition menus, etc.), followed by the definition of two 2D histograms, representing the mean intensities and standard deviation values of a 10x10 neighborhood for each image pixel. With the application of a Gaussian low-pass filter, kernel size of 40x40 pixels and σ=10, for speckle noise reduction, the combining of this information with the two 2D histograms will allow the identification of the lumen region of the carotid artery by its hipoechogenic characteristics. A signed distance function (SDF) is created, representing the distance map to the carotid lumen boundaries, with negative values inside the lumen region.

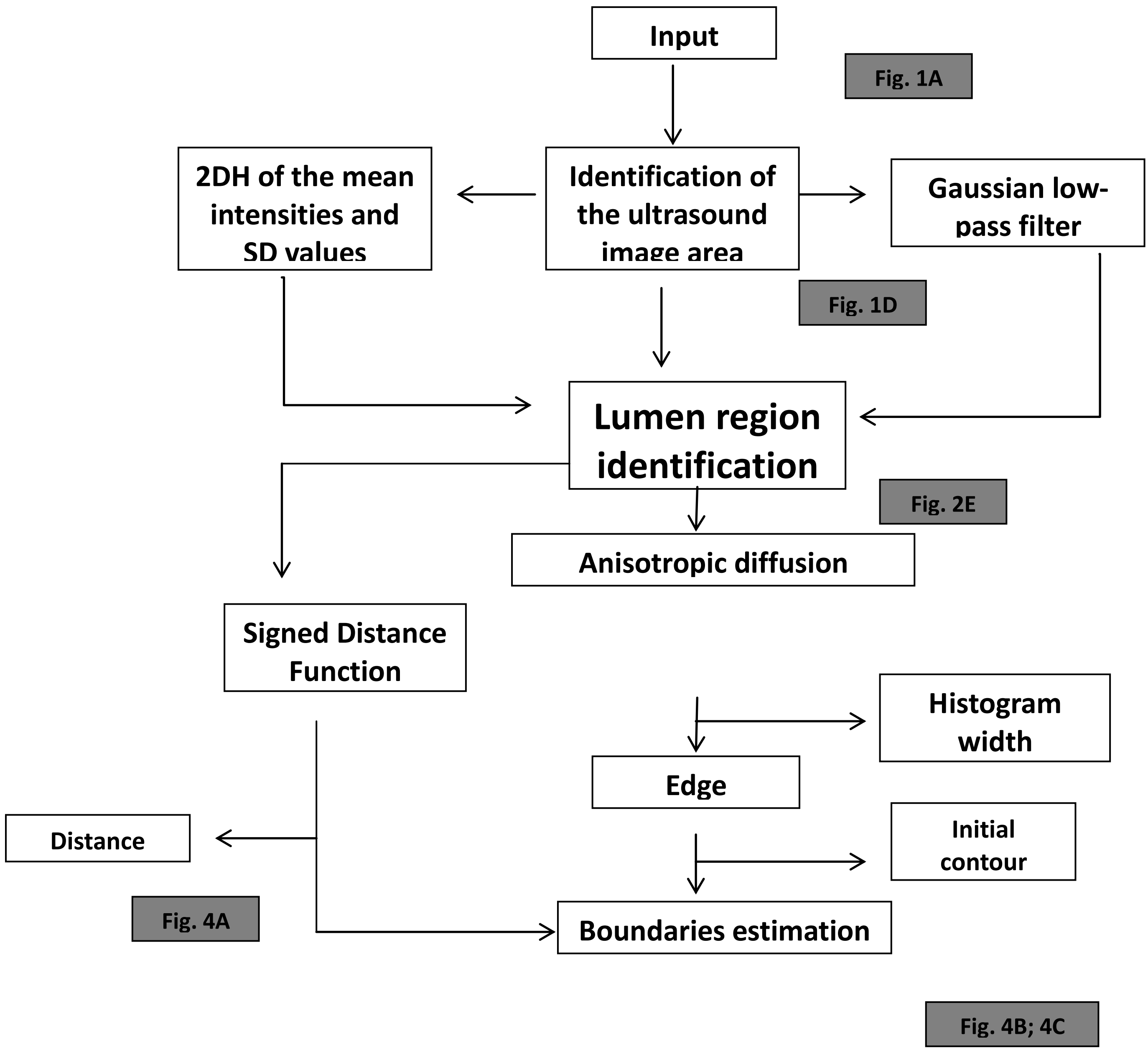

Figure 1: Main steps of the method developed.

The edges of the lumen and bifurcation of the carotid artery are detected, using an anisotropic diffusion filtering, histogram width threshold and Sobel operator application for edge detection. Afterwards, with the edge estimation information, two initial masks are created for the lumen and bifurcation boundaries identification. Combining these two masks with the SDF, two initial contours are defined in order to be used for the application of a geometric model, using the Chan-Vese energy minimization, for the identification of the lumen and bifurcation boundaries of the carotid artery.

Data set: A set of 5 longitudinal B-mode images of the CCA was acquired using a GE Healthcare Vivid-e ultrasound system, with 256 gray levels. All these images include a part of the CCA and the bifurcation that separates the CCA into the ICA and ECA. In order to achieve robustness in our acquisitions, with the highest contrast and lowest speckle noise levels as possible, the parameter settings of the scanner were different for each acquisition, according to the characteristics of each image.

Identification of the image area and consequent reduction of image size: As a first step, our goal is to reduce the image area, eliminating any possibility of detecting unwanted features, which did not belong to the ultrasound data. This procedure also reduces the time required for the performance of the posterior steps of image pre-processing and segmentation task. The reduction of the image area was based on the work developed by Golemati et al. (2007) and it consists on the definition of a rectangular area, involving the carotid artery. With this in mind, one proceeds with the definition of four points, based on the following procedure: (1) Morphological opening of the original image, based on a disk with a radius of 15 pixels, filtering unwanted structures such as letters; (2) Thresholding, replacing all pixels with luminance greater than 0.1 with the value 1 (corresponding to the white color in a binary image) and all others with 0 (black color), thus reducing the areas lying around the ultrasound image; (3) Finally, comes the definition of the four points, corresponding to the first and last nonzero lines and columns of the binary image. These four points will be the vertices of the rectangular area, where all the pre-processing and segmentation tasks will be performed.

Lumen region identification: This procedure was based on the study performed by Liboni et al. (2007), where it was developed a computer-based tracing of the carotid artery. According to Liboni et al. (2007), the carotid characteristics in an ultrasound image can be considered as a model of variable intensity distributions over the carotid's structure. It is precisely this ideology that is to be used in the automatic identification of the lumen of the carotid artery.

Pixels belonging to the lumen region of the carotid artery will be those characterized by both low mean and standard deviation values. In order to proceed with this identification, this step of our work was based in Liboni et al. (2007) method, with the construction of a 2D histogram. For each pixel of the cropped image, it was considered a 10x10 neighborhood, calculating for each one, the mean and standard deviation values. Both these values were posteriorly normalized and grouped into 50 classes with a 0.02 interval value. In our images, the results showed that lumen pixels had a mean intensity value belonging to the first five classes, while the standard deviation belonged to the first seven. Consequently, it was defined that a pixel of the cropped image would possibly belong to the lumen of the carotid artery if its 10x10 neighborhood intensity was lower than 0.1 and standard deviation below 0.14.

A row-wise intensity distribution graphic must be constructed for each column of the cropped ultrasound image, so one can identify the pixels corresponding to each frame of the carotid artery. However, before this step, the image must first pass through a pre-processing using a Gaussian low-pass filter, kernel size of 40x40 pixels and $\sigma=10$, for speckle noise and attenuating high intensity noisy points of the intensity distribution. Afterwards, during the processing it was considered that the top row of the cropped would correspond to the lowest row, while the bottom one would correspond to the lowest. As mentioned previously, pixels belonging to the lumen region of the carotid artery are those characterized by their low mean intensities and standard deviation values. Having this into consideration, those pixels can be identified in the intensity distribution graphics as being those correspond to the minimum values of that graphic, and usually between local maxima, corresponding to the near and far adventitia layers, or corresponding to the walls of the ICA and ECA, or even in the interval between these two frames, if it is considered a column of the image containing pixels belonging to the carotid bifurcation. As such, and based on Liboni et al. (2007) method, it was chosen to start the identification process from the bottom of the cropped image (highest row value) and will moving upwards along the row, decreasing the row value in, order to correctly identify the first pixel of the first maxima as possibly corresponding to the far adventitia of the carotid, usually associated to the brightest frame of the ultrasound image of the carotid artery. Having the estimation of this first pixel, as possibly belonging to the far adventitia, for the lumen identification, the algorithm continues moving upwards and searching for a pixel possible belonging to the lumen region. Taking into account the row of the pixel corresponding to the far adventitia, the pixel possibly belonging to the lumen will be the first minima point after the far adventitia pixel. Also, its neighborhood mean intensity and standard deviation, must match the chosen criteria of the 2D histogram, with a 10x10 neighborhood mean intensity and standard deviation lower than 0.1 and 0.14, respectively.

Lumen edges identification: Having the correct identification of a class of pixels belonging to the lumen of the carotid artery, the construction of a suitable mask for a level set segmentation is now possible. First, a few processing techniques must be applied to the cropped image, in order to raise the robustness of our algorithm in the mask construction. Initially, a conventional anisotropic diffusion filter must be applied to the image, in order to attenuate the great amount of speckle noise that is present in the image. For this step, it was chosen the filter proposed in (Perona and Malik, 1990) with a 2D network structure of 8 neighboring nodes for diffusion conduction. Then, it is applied of a morphological closing operator to the image, merging small “channels” and “openings”. Thirdly, it was performed a threshold based on the image’s histogram width, using the value corresponding to its first 15%. This threshold will result in a binary image, on which is applied the Sobel gradient operator in order to identify the edge points. The posterior result of this edge detection is also a binary image having 1s at edge locations. The binary image acquired with the application of the Sobel gradient operator, combined with the information relevant to the pixels that belong to the lumen region of the carotid, will allow the identification of the edges correspondent to the superior and inferior wall of the lumen of the carotid artery. Figure 2E shows that combination, where it can be considered the pixel of the lumen candidates string with the highest column value (placed more to the right of the image), and it can be searched in the binary image resulted from the Sobel operator application, the pixels above and below (in the same column) with value 1 (one). Having the row and column of these two pixels, one belonging to the superior lumen edge and the other to the inferior one, it is possible to trace the rest of the edge in the Sobel binary image and save the coordinates of each pixel in a string. As a result, two strings are originated, having the coordinates of each pixel belonging to the superior and inferior lumen edges. Posteriorly, the definition of a new string takes place, containing the pixels belonging to the bifurcation edge in the binary image, knowing that the bifurcation is localized between the superior and inferior walls of the carotid. Finally, it is processed to the definition of two different masks, for posterior application of the geometrical model of Chan-Vese for the segmentation of both bifurcation and common carotid artery walls, as shown in Figure 4.

Segmentation of the lumen and bifurcation boundaries of the carotid artery, using the Chan-Vese geometrical model: Using the two masks created in the previous step, as initial contours, the Chan-Vese level set becomes a powerful segmentation method to detect the lumen boundaries of the carotid artery. It is known for its great flexibility and accuracy as a region-based model and independent of gradients. This independence makes the segmentation extremely robust in cases of small gaps in the boundaries of the carotid. The segmentation performed on both the lumen and bifurcation boundaries of the carotid artery is based on the work developed by Lankton and Tannenbaum (2008) where it was defined a local-based framework, where the active contour moves according to an internal energy, defined by Chan and Vese , using a constant intensity model. The framework starts with the input of an initial contour (in this case, it is chosen one of the masks created in the previous step, and a signed distance function (SDF) is created, based on the following equation:

$$\phi = E_d(m) - E_d(1-m) + \left(m - \left(\tfrac{1}{2}\right)\right), \quad (1)$$

where ϕ is SDF, m represents the initial contour as a binary image and E_d is the Euclidean distance transform of a considered binary image, assigning for each pixel, the distance between them and the nearest nonzero value. The Euclidean distance between two points (x_1, y_1),(x_2, y_2), is given by:

$$E = \sqrt{(x_1 - x_2)^2 + (y_1 - y_2)^2}, \quad (2)$$

where C represents a closed contour as the zero level of SDF, i.e., $C = \{x | SDF(x) = 0\}$, which interior and exterior will be expressed respectively by:

$$H\,\phi(x) = \begin{cases} 1 & , \phi(x) < -\epsilon \\ 0 & , \phi(x) > \epsilon \\ \frac{1}{2}\left\{1 + \frac{\phi}{\epsilon} + \frac{1}{\pi}\sin\left(\frac{\pi\phi(x)}{\epsilon}\right)\right\} & , otherwise \end{cases}, \quad (3)$$

$$\phi(x) = [1 - H\,\phi(x)]. \quad (4)$$

The area surrounding C, just in its neighborhood, is specified by derivating equation (3):

$$\delta\,\phi(x) = \begin{cases} 1, & \phi(x) = 0 \\ 0, & |\phi(x) < \epsilon| \\ \frac{1}{2\epsilon}\left\{1 + \cos\frac{\pi\,\phi(x)}{\epsilon}\right\}, & otherwise \end{cases}, \quad (5)$$

Considering x and y as independent variables, representing the coordinates of a single point in the domain Ω of an ultrasound image, the following equation represents a function defining a circular region of interest (ROI) of radius r and center x, with value 1 (one) inside and 0 (zero) outside:

$$B(x,y) = \begin{cases} 1, & \|x - y\| < r \\ 0, & otherwise \end{cases}. \quad (6)$$

With eq. (6), the energy functional can finally be defined as:

$$E(\phi) = \int_{\Omega_x} \delta\,\phi(x) \int_{\Omega_y} B(x,y).F\big(I(y),\phi(y)\big)\,dy\,dx. \quad (7)$$

In this equation, $\delta\,\phi(x)$ prevents the development of new contours, ensuring that C does not undergo sudden changes in its geometry. On the other hand, it will allow certain parts of the contour C to separate or combine within each other. Each point x in this term, it is masked to $B(x,y)$ ensuring that only the local information surrounding C will be used.

The smoothness of the contour C curve is kept, through the application of a new regularization term, penalizing its arc length. The weight of this penalty is controlled by the parameter λ in the new equation of the energy functional:

$$E(\phi) = \int_{\Omega_x} \delta\ \phi(x) \int_{\Omega_y} B(x,y).F\big(I(y),\phi(y)\big)\,dy\,dx + \lambda \int_{\Omega_x} \delta\,\phi(x)\|\nabla\,\phi(x)\|\ dx \quad (8)$$

Next, Lanktom and Tannenbaum (Lanktom and Tannenbaum, 2008) tested the introduction of specific energies to the generic framework described previously, including the Chan-Vese energy, expressed by the equation:

$$E_{CV} = \int_{\Omega_y} H\,\phi(y)(I(y)-u)^2 + \big(1-H\,\phi(y)\big)(I(y)-v)^2\ dy, \quad (9)$$

where u and v are global mean intensities of the interior and exterior of *C* and from which the modeling of the contour is based. These global mean intensities are given by:

$$u = \frac{\int_{\Omega_y} H\,\phi(y).I(y)\,dy}{\int_{\Omega_y} H\,\phi(y)\,dy}, \quad (10)$$

$$v = \frac{\int_{\Omega_y} \big(1-H\,\phi(y)\big).I(y)\,dy}{\int_{\Omega_y} \big(1-H\,\phi(y)\big)\,dy}. \quad (11)$$

The corresponding internal energy function of the Chan-Vese energy is based in the local mean intensities u_x and v_x, instead of u and v:

$$F_{CV} = H\,\phi(y)(I(y)-u_x)^2 + \big(1-H\,\phi(y)\big)(I(y)-v_x)^2, \quad (12)$$

$$u_x = \frac{\int_{\Omega_y} B(x,y)\,H\,\phi(y).I(y)\,dy}{\int_{\Omega_y} B(x,y)\,H\,\phi(y)\,dy}, \quad (13)$$

$$v_x = \frac{\int_{\Omega_y} B(x,y)\big(1-H\,\phi(y)\big).I(y)\,dy}{\int_{\Omega_y} B(x,y)\big(1-H\,\phi(y)\big)\,dy}. \quad (14)$$

Equation (12) can now be substituted in the energy functional of the framework (eq. (8)), defining a localized energy. To obtain the curvature's flow regularization term, equation (12) must first be derivated and substituted in equation (8), as demonstrated below in equations (15) and (16), respectively:

$$\nabla_{\phi(y)}F = \delta\,\phi(y)\big((I(y)-u_x)^2 - (I(y)-v_x)^2\big), \quad (15)$$

$$\frac{\partial\phi}{\partial t}(x) = \delta\,\phi(x)\int_{\Omega_y} B(x,y)\ \nabla_{\phi(y)}F\big(I(y),\phi(y)\big)\,dy + \lambda\,\delta\,\phi(x)\ div\left(\frac{\nabla\phi(x)}{|\nabla\phi(x)|}\right) \Leftrightarrow$$

$$\frac{\partial\phi}{\partial t}(x) =$$

$$\delta\,\phi(x)\int_{\Omega_y} B(x,y)\ \delta\,\phi(y)\big((I(y)-u_x)^2 - (I(y)-v_x)^2\big)\,dy + \lambda\,\delta\,\phi(x)\ div\left(\frac{\nabla\phi(x)}{|\nabla\phi(x)|}\right) \quad (16)$$

The Chan-Vese energy function finds its minimum when the interior and exterior of the curve are closer to the global mean intensities u and v, while in the localized version the minimum is obtained when they are closer to the local mean intensities u_x and v_x.

For the segmentation of the bifurcation boundaries, the mask illustrated in Figure 3g was chosen as the initial contour. The level set for the segmentation of these boundaries must be flexible in order to reach the limit of the bifurcation walls, so in this case, for the penalty of the arc length of the contour *C*, a control parameter λ of value 0.3 and a circular ROI u_x and $B(x,y)$ of 5 pixels radius were chosen. On the other hand, for the segmentation of the lumen boundaries, the mask illustrated in Figure 3f was selected and the control parameter λ of the penalty of the arc length of *C* was higher $(\lambda = 0.6)$, since the development contour *C* has to be properly controlled and somehow attenuated, in order to prevent its development towards other structures or vessels near the carotid artery. The circular ROI $B(x,y)$ was also chosen to be smaller, this time with a radius of only 1 pixel, to prevent larger intensity variations during the contour *C* development with the Chan-Vese energy minimization.

Contour smoothness: Finally, as a final step, the obtained contours must be smoothed. In this procedure, the contour smoothing is done: Firstly, through a cubic spline interpolation and secondly, by projecting all the resulting points of the contour towards the local regression line. Once again, for each point of the contour, a ROI is defined, defining the number of points in the neighborhood of the contour that will contribute for the computation of the local regression line. In this procedure, for each pixel of the contour there is the definition of an 8-connected-neighborhood pixel for this computation.

RESULTS

A complete demonstration of the approaches described in the previous sections, which compose our method, is represented in Figures 2, 3, 4 and 5.Figure 2, shows an example of the first procedure aiming to identify automatically a rectangular area enclosing the ultrasound environment of the input image.

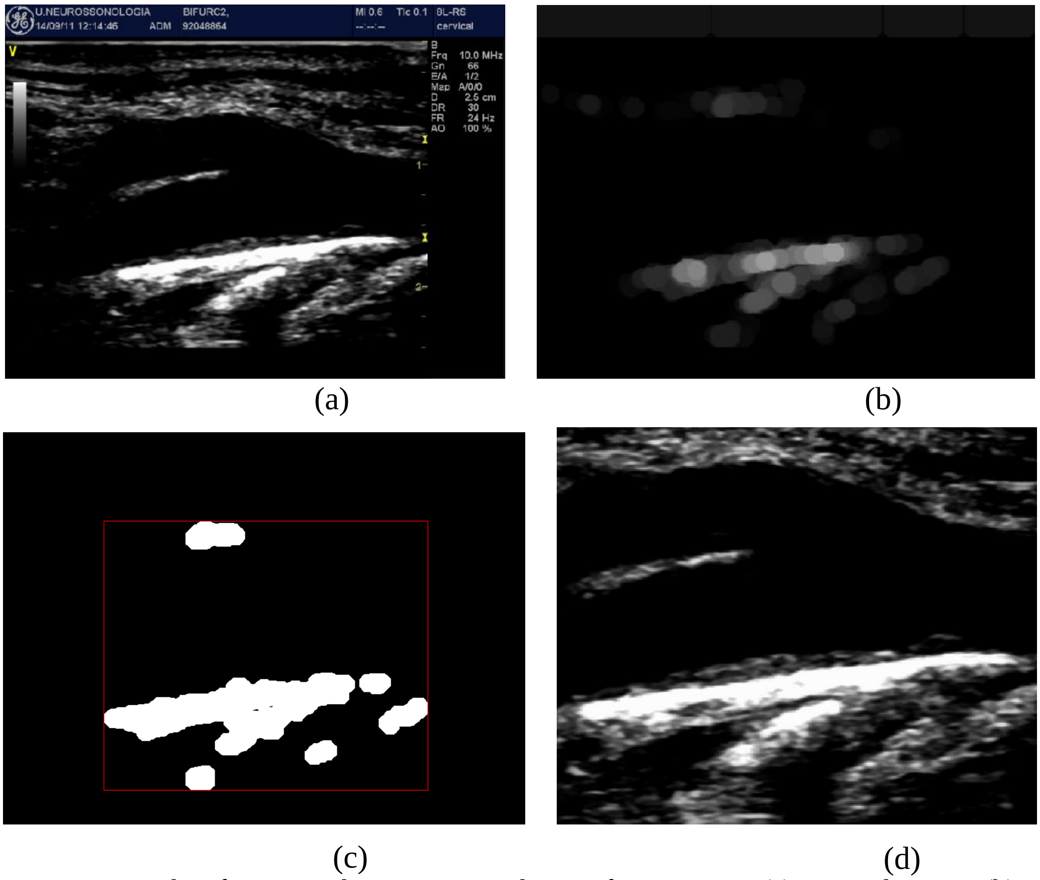

Figure 2: Automatic identification and consequent isolation of image area: (a) Original image; (b) After the morphological opening; (c) After Thresholding, and definition of a rectangular area, based on the first and last nonzero lines and columns; (c) Resulted image.

Figure 3 shows an example of the identification of the lumen region of the CCA, in one of the acquired ultrasound images of the carotid artery. Figures 3a and 3b illustrate the 2D histogram of the mean intensities and standard deviation values according to the 50 classes from which the standard deviation and mean values corresponding to the two 2D histograms were grouped, from which they were separated; Figure 3c illustrates the cropped image after the application of the Gaussian low-pass filter; All the possible pixel candidates for the lumen region of the CCA are represented by the value 1 (white color) in a binary image in Figure 3d; Finally, Figure 3e illustrates the pixels that were identified as belonging to the lumen region of the CCA and as being closer to the lumen boundaries of the CCA and which will be used in the definition of the initial contour for the application of the Chan-Vese algorithm.

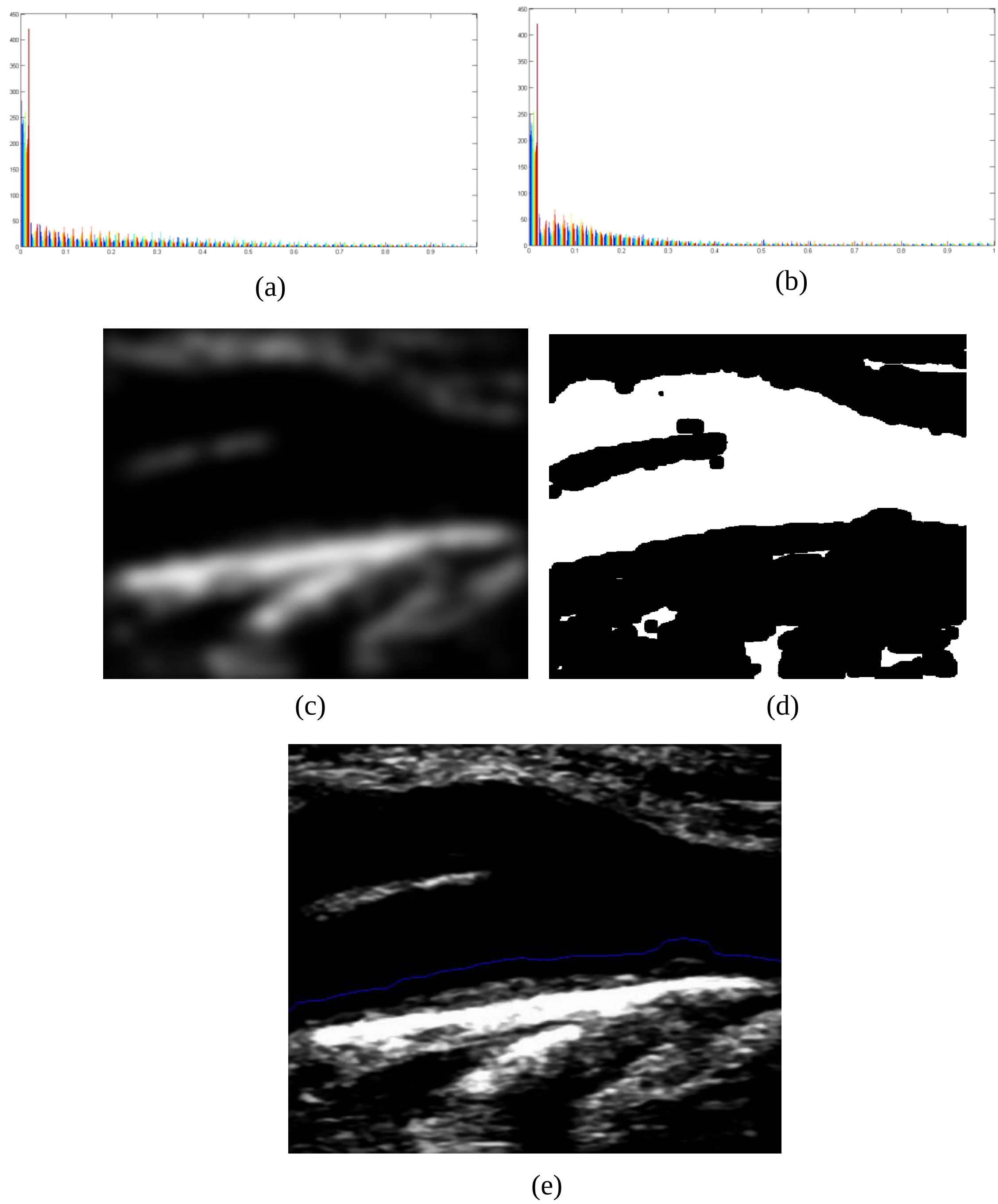

Figure 3: Automatic identification of the lumen region of the CCA in one of the acquired ultrasound images of the carotid artery (a); (b) 2D histogram representation of each pixel 7x7 neighborhood mean intensities and standard deviations, separated in 50 different classes with a 0.02 value interval; (c) Cropped image after the application of a Gaussian low-pass filter, with kernel size of 40x40 pixels and σ=10; (d) Binary image with the illustration of all possible pixel candidate for the lumen region of the CCA with value 1 (white color); (e) Cropped image, with the pixels identified as belonging to the lumen of the CCA in blue color.

Figure 4 despites all the described procedures used for the identification of the lumen edges. Figure 4a illustrates the cropped image in double (intensities from 0 to 255, corresponding 0 to the black and 255 to white), while Figure 4b illustrates the same image after the application of the anisotropic filter proposed by Perona and Malik (1990) for speckle removal. After the threshold based on the first 15% of the histogram width, the image illustrated in Figure 4c is obtained and with the application of the Sobel operator for edge detection, it is obtained the image illustrated in Figure 4d. Figure 4e illustrates in green, the pixels detected in the binary image after the Sobel operator application as belonging to the superior and inferior walls of the carotid artery and to its bifurcation. Finally, Figures 4f and 4g illustrate the two masks that will serve as an input for the definition of an initial contour in the Chan-Vese level set segmentation.

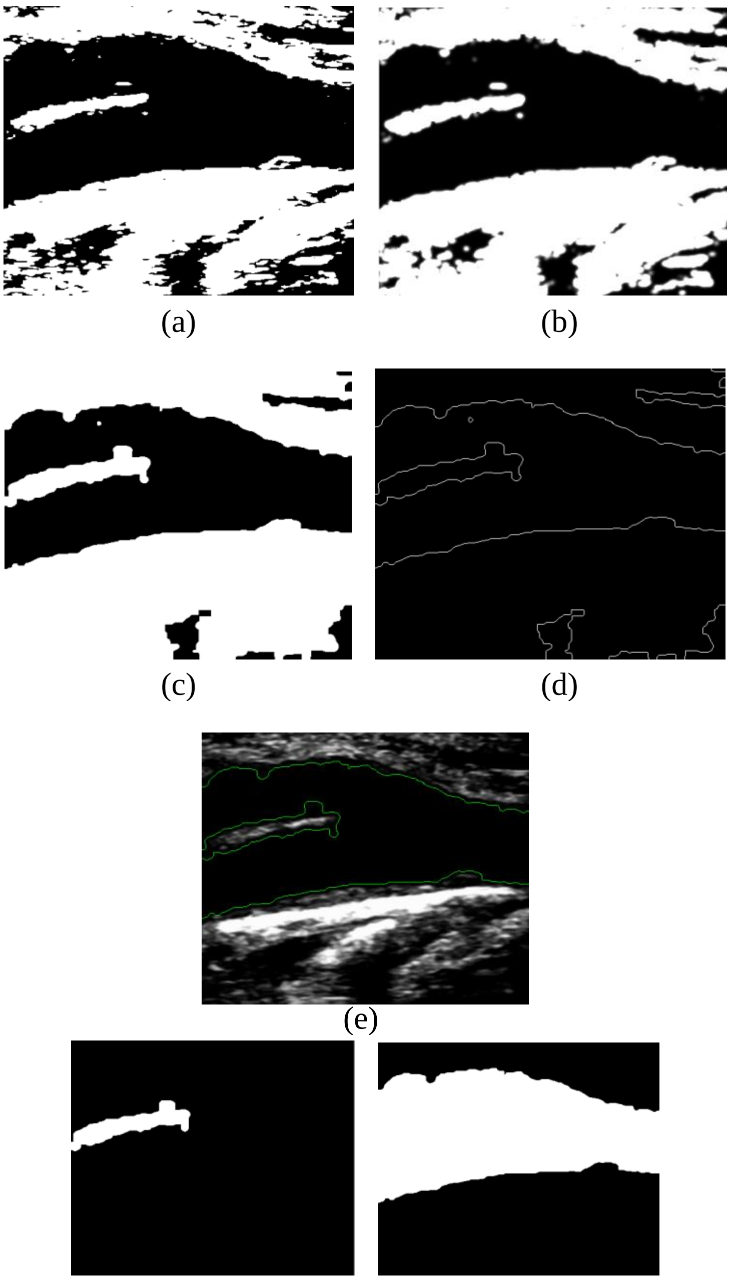

(a) (b)

(c) (d)

(e)

(f) (g)

Figure 4: Lumen edges identification: (a) Cropped image in double; (b) Resulted image after the application of an anisotropic diffusion filter for speckle removal; (c) Threshold based on the first 15% of the image's histogram width; (d) Sobel operator for edge detection; (e) Cropped image, where there can be identified in green, the pixels detected in the binary image after the Sobel operator application as belonging to the superior and inferior walls of the carotid artery; (f and g) Two binary images, defining the masks, based on the information of the lumen walls and the bifurcation of the carotid artery.

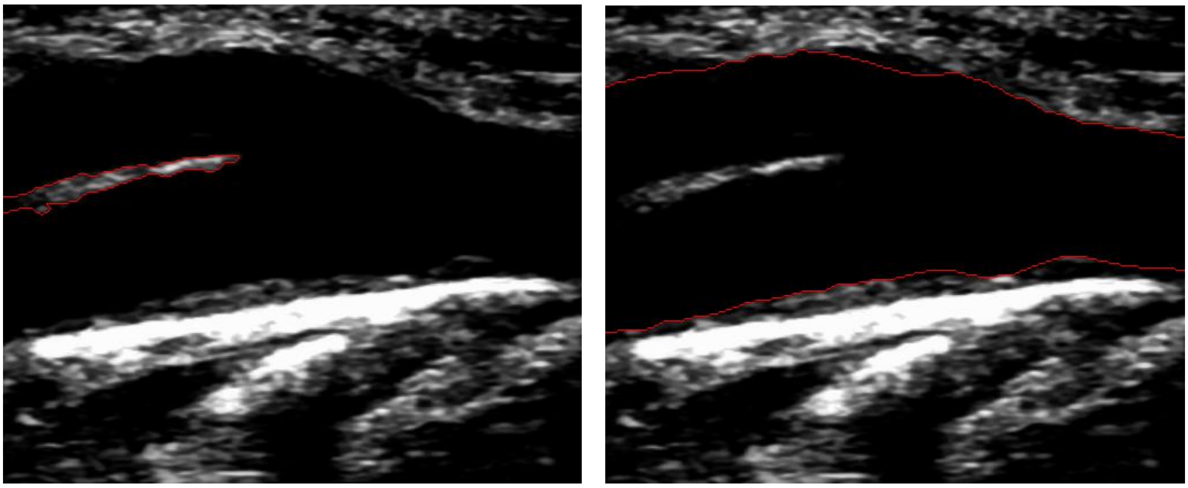

(a) (b)

Figure 5: Geometric model level set using the Chan-Vese energy minimization: (a) Identification of the bifurcation boundaries of the carotid artery; (b) Identification of the lumen boundaries of the carotid artery.

The smoothed contours of the lumen and bifurcation boundaries are combined in the same image, and the result is illustrated in Figure 6.

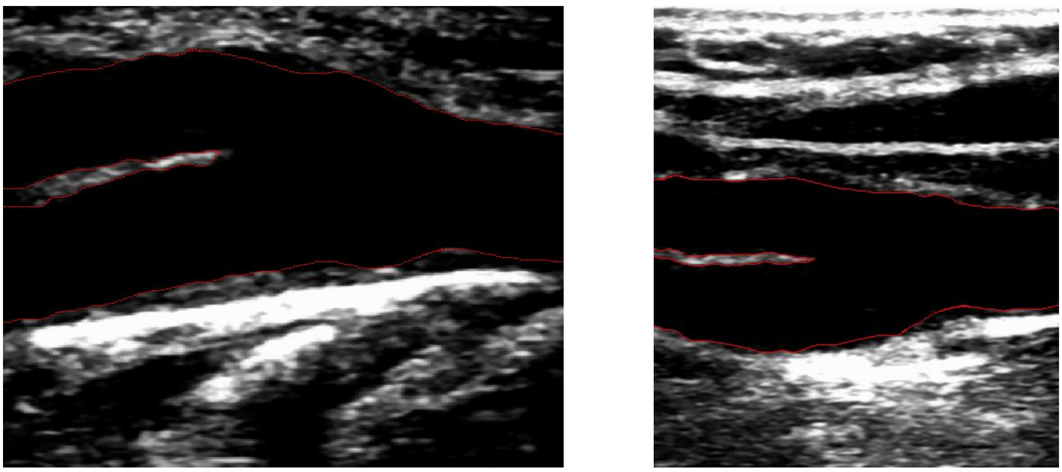

(a) (b)

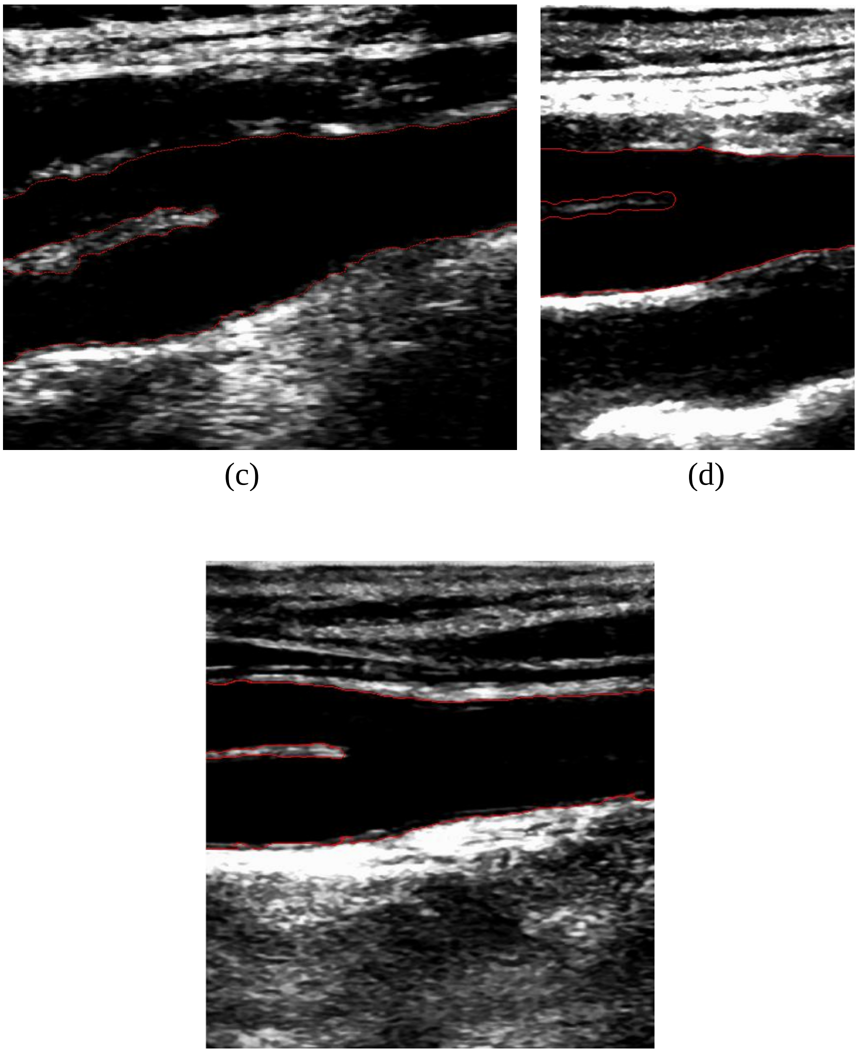

(c) (d)

(e)

Figure 6: Identification of lumen and bifurcation boundaries of the carotid artery. Each image illustrates the carotid artery of a different ultrasound acquisition for each one of the tested healthy subjects

DISCUSSION

The proposed method provides a fully automatic segmentation of the arterial lumen and bifurcation sections of the carotid artery in longitudinal ultrasound images. Its main advantage relies on the automatic identification of the carotid lumen, through its hipoechogenic characteristics, overcoming the limitations of traditional methods.

As showed in Figure 4b, the application of the anisotropic diffusion filter developed by Perona and Malik (1990) was satisfactory, allowing the correct distinction of the carotid artery from other near vessels and small features, which greatly facilitated the detection of the boundaries of the carotid for the definition of a initial contour for the application of the Chan-Vese energy model.

In the tested images, the initial contour of the Chan-Vese model has been successfully set, very close to the true lumen and bifurcation boundaries of the carotid artery, which is an advantage in the proposed method, since it greatly increases the robustness of the segmentation procedure.

Regarding the results of the proposed method, illustrated in Figure 6, we can consider them to be satisfactory. As it can be seen in the images presented, in general, there was a correct targeting and segmentation of the boundaries of the lumen and bifurcation of the carotid artery. The segmentation with the greatest degree of success was the one illustrated in Figure 6a, since although it is the case where the lumen, intima-media and adventitia boundaries are best defined in terms of contrast, hipoechogenic characteristics and noising, the contours that were obtained are highly smoothed, picturing perfectly the surface of the carotid artery. The bifurcation is also very well defined in this image. The same is not happening, for example, in the carotid illustrated in Figure 6d, where it is clear that the contrast of the bifurcation of this carotid artery is really very poor and with a high level of noise and gaps in its interior. Both this case and others where the boundaries of the lumen are not well defined and with higher noise level, due to the difficulty in acquiring good images during an ultrasound acquisition, represent the next steps of our work, where it will be improved the segmentation robustness of the proposed method, taking into account these weaknesses for a greater number of images of carotid arteries, with different structures, for both normal and patients with atherosclerosis. Then, the manual segmentation by a specialist will be performed, for the statistical comparison with the automatic segmentation and posterior validation of the algorithm, in order to proceed to the 3D modeling of these carotid arteries.

CONCLUSIONS

We were able to successfully apply a carotid segmentation method on cervical ultrasonography images. The main advantage of our segmentation method relied on the automatic identification of the carotid lumen, overcoming the limitations of traditional methods.

In the future, we will proceed to the 3D modelling of the carotid. These 3D models will be important for testing hypotheses and address practical clinical vascular problems related to carotid diseases.

ACKNOWLEDGMENTS

This work was done in the scope of the projects “Methodologies to Analyze Organs from Complex Medical Images – Applications to Female Pelvic Cavity”, “Blood flow simulation in arterial networks towards application at hospital” and “Cardiovascular Imaging Modeling and Simulation - SIMCARD”, with references PTDC/EEA-CRO/103320/2008, PTDC/SAU-BEB/102547/2008 and UTAustin/CA/0047/2008, respectively, financially supported by Fundação para a Ciência e a Tecnologia (FCT) in Portugal.

REFERENCES

Abdel-Dayem AR, El-Sakka MR. 2005. Carotid artery image segmentation using fuzzy region growing. International Conference of Image Analysis and Recognition. Toronto, Canada. vol. 3656. pp 869-878;

Abdel-Dayem AR, El-Sakka MR. 2005. Carotid artery contour extraction from ultrasound images using multi-resolution analysis and watershed segmentation scheme. Graphics, Vision and Image Processing. Cairo, Egypt;

Antiga L, Ene-Irodache B, Remuzzi A. May 2003. Computational geometry for patient-specific reconstruction and meshing of blood vessels from MR and CT angiography. IEEE Transactions on medical imaging. vol. 22. nº 5. pp 674-684;

Barratt DC, Ariff BB, Humphries KN, Thim SAM, Hughes AD. May 2004. Reconstruction and quantification of the carotid artery bifurcation from 3D ultrasound images. IEEE Transaction on medical imaging. vol. 23. nº 5. pp. 567-583;

Chan KL. 1993. Ultrasound tissue characterization using fractal feature. IEEE conference of acoustic sensing and imaging. nº 369. pp. 193-188;

Chen Y, Huan HD, Tagare HD, Rao M, Wilson D, Geiser EA. 2003. Using prior shape and intensity profile in medical image segmentation. IEEE international conference of computational vision. vol. 2. pp 1117-1125;

Cheng DC, Billich C, Liu SH, Qiu YC, Shen YL, Brambs HJ, Trucksass AS, Schutz UHW. 2011. Automatic detection of the carotid artery boundary on cross-sectional MR image sequences using circle model guided dynamic programming. Biomedcial Enginerring Online. pp 10-26;

Cheng D, Schmidt-Trucksass A, Cheng K, Sandrock M, Pu Q, Burkhardt H. 1999. Automatic detection of the intimal and the adventitial layers of the common carotid artery wall in ultrasound B-mode images using snakes. International conference on image analysis and processing. pp 452-457;

Cheng D, Schmidt-Trucksass A, Cheng K, Sandrock M, Pu Q, Burkhardt H. 2002. Using snakes to detect the intimal and adventitial layers of the common carotid artery wall in sonographic images. Computer methods and programs in biomedicine. vol. 67. pp 27-37;

Cheng J, Ding M, Zhang X. 2011. Geometric active contour model and its application to carotid plaque detection. International conference computation and biomedical instrumentation;

Chiu B, Beletsky V, Spence JD, Parrag G, Fenster A. 2009. Analysis of carotid surface morphology using three-dimensional ultrasound imaging. Phys. Med. Biol. vol. 54. pp 1149-1167;

Cremers D, Kohlberger T, Shcorr C. 2002. Nonlinear shape statistics in Mumford-Shah based segmentation. Proc. European conference on computer vision. Copenhagen. vol. 2351. pp 93-108;

Cremers D, Osher S, Soatto S. 2004. Kernel density estimation and intrinsic alignment for knowledge-driven segmentation: teaghing level sets to walk. Pattern recognition. vol. 3175. pp 36-44;

Cremers D, Sochen N, Schnorr C . 2003. Towards recognition-based variation segmentation using shape prior and dynamic labeling. Proc European conference on computer vision. vol. 2685. pp 388-400;

De Santis G, Mortier P, De Beule M, Segers P, Verdonck P, Verhegge B. 2010. Patient-specific computational fluid dynamics: structured mesh generation from coronary angiography. Med Biol Eng Comput. vol.48. pp 371-380;

Dutt V, GrennLeaf. 1994. Ultrasound echo envelope analysis using a homodyned k-distribution signal model. Ultrasound imaging. vol. 16. pp 365-387;

Gariepy J, Massonneau M, Levenson J, Heudes D, Simon A. 1993. Evidence for in vivo carotid and femoral wall thickness in human hypertension. J. Hypertension. vol. 22. nº1. pp 111-118;

Golemati S, Stoitsis J, Sifakis EG, Balkizas T, Nikita KS. 2007. Using the hough transform to segment ultrasound images of longitudinal and transverse sections of the carotid artery. Ultrasound in Med & Biol. vol. 33. nº 12. pp 1918-1932;

Gustavsson T, Liang Q, Wendelhag I, Wikstrand J. 1994. A dynamic programming procedure for automated ultrasonic of the carotid artery. Computers in cardiology. pp 297-300;

Haneline MT, Croft AC, Frishberg BM. 2003. Association of internal carotid artery dissection and chiropractic manipulation. The neurologist. vol. 9. pp 35-44;

Izquierdo-Zaragoza, JL, Bastida-Jumilla MC, Verdú-Monedero R. 2011. Segmentation of the carotid artery in ultrasound images using frequency-designed b-spline active contour. ICASSP. pp. 713-716;

Jegelevicius D, Lukosevicius A. 2002. Ultrasonic measurements of human carotid artery wall intima-media thickness. ULTRAGARSAS. nº 2. vol. 43;

Jiaoying J, Mingyue D, Yang X. 2011. Automatic detection of the intima-layer in ultrasound common carotid artery image based on active contour model. Intelligent Computation and Bio-Medical Instrumentation (ICBMI). DOI 10.1109/ICBMI348. pp 105-108;

Kozich RJ. 1996. Detecting interfaces on ultrasound images of the carotid artery by dynamic programming. SPIE. vol. 2666. pp 233-241;

Lanktom S, Tannenbaum A. 2008. Localizing Region-Based Active Contours. IEEE Transaction on image processing. vol. 17. nº11. pp 2029-2038;

Loizou CP, Pattichis CS, Pantziaris M. November 2007. An integrated system for the segmentation of atherosclerosis carotid plaque. IEEE Transactions on information technology in biomedicine. vol. 11. nº 6. pp. 661-667;

Matsakou AI, Golemati S, Stoitsis JS. 2011. Automated detection of the carotid artery wall in longitudinal B-mode images using active contours initialized by the hough transform. 33rd annual international conference of the IEEE EMBS. Boston. Massachusetts USA. August 30-September 3;

Meiburguer KM, Molinari F, Acharya UR, Saba L, Rodrigues P, Liboni W, Nicholaides A, Suri JS. 2011. Automated carotid artery intima-layer regional segmentation. Physics in medicine and biology. vol. 56. pp 4073-4090;

Milner JS, Moore JA, Rutt BK, Steinman DA. 1998 Hemodynamics of human carotid artery bifurcation: computational studies reconstructed from magnetic resonance imaging of normal subjects. Journal of vascular surgery. vol.28. nº1. pp.143-156;

Molinari F, Liboni W, Giustetto P, Badalamenti S. 2009. Automated computer-based tracings (ACT) in longitudinal images using different scanners. Journal of mechanics in medicine and biology. vol. 9. pp 1-25;

Molinari F, Liboni W, Giustetto P, Suri JS. August 23-26. 2007. Accurate and automatic carotid plaque characterization in contrast enhanced 2D ultrasound images. Proceedings of the 29th annual international conference of the IEEE EMBS. Lyon. France;

Molinari F, Zeng G, Suri JS. 2010. An integrated approach to computer based automated tracing and its validation for 200 common carotid artery Wall ultrasound Wall images. Journal of Ultrasound in Medicine. vol.29. nº3. pp 399-418;

Molthen RC, Narayanan VM, Shankar PM, Reid JM, Genis V, Vergara-Domínguez L. 1993. Ultrasound echo evaluation by k-distribution. Ultrasonics symposium. IEEE. pp 957-960;

Nambi V, Chambless L, He M, Folsom AR, Mosley T, Boerwinkle E, Ballantyne CM. 2012. Common carotid artery intima-media thickness is as good as carotid intima-media thickness of all carotid artery segments in improving prediction of coronary heart disease risk in atherosclerotic risk in communities (ARIC) study. European Heart Journal. vol. 33. pp 183-190;

Noble JA, Boukerrouni D. 2006. Ultrasound image segmentation: a survey. IEEE Transaction in medical imaging. vol. 25. nº 8. pp 987-1010;

Osher S, Fedwik R. 2003. Level set methods and dynamic implicit surfaces. Springer-Verlag. New York;

Perona P, Malik J. July 1990. Scale-space and edge detection using anisotropic diffusion. IEEE transaction on pattern analysis and machine intelligence. vol. 12. nº 7. pp.629-639;

Petroudi S, Loizou C, Pantziaris M, Pattichis M, Pattichis CS. 2011. A fully automated method using active contours for the evaluation of the intima-media thickness in carotid US images. 33rd annual international conference of the IEEE EMBS. Boston, Massachusetts USA;

Petroudi S, Loizou CP, Pattichis CS. 2010. Atherosclerosis carotid Wall segmentation in ultrasound images using markov random fields. IEEE Transactions in Medical Imaging. vol. 978. nº1. pp. 1-5;

Poonguzhali S, Ravindran G. 2006. A complete automatic region growing method for segmentation of masses on ultrasound images. Research Publishing Services;

Rocha R, Campilho A, Silva J. 2005. Segmentation of ultrasonic images of the carotid. ICIAR 2005 LNCS 3656. pp 949-957;

Rocha R, Campilho A, Silva J, Azevedo E, Santos R. 2008. Segmentation of the carotid intima-media region in B-mode ultrasound images. Image and vision computing. vol.28. pp 614-625;

Rocha R, Campilho A, Silva J, Azevedo E, Santos R. 2011. Segmentation of ultrasound images of the carotid using RANSAC and cubic splines. Computer methods and programs in biomedicine. vol. 101. pp 94-106;

Rossi AC, Brands PJ, Hoeks APG. 2008. Automatic recognition of the common carotid artery in longitudinal ultrasound B-mode scans. Medical image analysis. vol. 12. pp 653-665;

Sanderse M, Marquering HA, Hendriks, EA, van der Lugt A, Reiber JHC. 2005. Automatic initialization algorithm for carotid artery segmentation in CTA images. MICCAI. LNCS 3750. pp 846-853;

Sarti A, Corsi C, Mazzini E, Lamberti C. 2004. Maximum likehood segmentation with rayleigh distribution of ultrasound images. Computers in cardiology. vol. 31. pp 329-332;

Schmidt-Trucksass A, Cheng D, Sandrock M, Schulte-Monting J, Rauramaa R, Huonker M, Burkhardt H. 2001. Computerized analyzing system using the active contour in ultrasound measurement of carotid artery intima-media thickness. Clinical Physiology. vol. 5. pp 561-569;

Selzer RH, Hodis, HN, Kwong-Fu H, Mack WJ, Lee PL, Liu CR, Liu CH. 1994. Evaluation of computerized edge tracking for quantifying intima-media thickness of the common carotid artery from B-mode ultrasound images. Atherosclerosis. vol. 1111. pp 1-11;

Sommer G, Holzapfel GA. 2012. 3D constitutive modeling of the biaxial mechanical response of intect and layer-dissected human carotid arteries. Journal of the mechanical behavior of biomedic materials. vol. 5. pp 116-128;

Thijssen JM. 2003. Ultrasonic speckle formation and processing applied to tissue characterization. Pattern recognition. vol. 24. nº 4-5. pp 659-675;

Thwin SS, Soe MM, Myint M, Lwin S. 2010. Variation of the origin and branches of the external carotid artery in human cadaver. Singapoore Med J. vol. 51(2). pp 40-42;

Touboul PJ, Prati P, Sxarabin PY, Adrai V, Thibout E, Ducimetiere P. 1992. Use of monitoring software to improve the measurement of carotid wall thickness by B-mode imaging. J. hypertension. vol. 10, nº 5. pp 37-41;

Unal G, Bucher S, Carlier S, Slabaugh G, Fang T, Tanaka K. May 2008. Shape-driven segmentation of the arterial wall in intravascular ultrasound images. IEEE Transaction on information technology in biomedicine. vol. 12. nº 3. pp 335-347;

Urquiza SA, Blanco PJ, Vénere MJ, Feijóo RA. 2004 Multidimensional modelling for the carotid artery blood flow. Computer methods in applied mechanics and engineering. pp. 1-18;

Vukadinovic D, van Walsum T, Manniesing R, Rozie S, Hameeteman R, de Weert TT, Lugt A, Niessen WJ. 2010. Segmentation of the outer wall of the common carotid artery in CTA. IEEE Transactions on medical imaging. vol. 9. nº1. pp. 65-75;

Wan J, Ruan Q, Li W. 2010. Using two methods for recognition common carotid artery of B-mode longitudinal ultrasound image. ICSO2010 Proceedings. IEEE;

Wagner RF, Smith SW, Sandrik JM, Lopez H. 1983. Statistical of speckle in ultrasound B-scans. IEEE Transaction. vol. 30. pp 156-163;

Yang X, Ding M, Lou L, Yuchi M, Qiu W, Sun Y. 2011. Common carotid artery lumen segmentation in B-mode ultrasound transverse view images. I.J. Image. Graphics and Signal Processing. vol. 5. pp 15-21;

Younis HF, Kaazempur-Mofrad MR, Chan RC, Isase AG, Hinton AH, Kin LA, Kamm RD. 2004. Hemodynamics and wall mechanics in human carotid bifurcation and its consequences for atherogenesis: investigation of inter-individual variation. Biomechan Model Mechanobiol. vol. 3. pp 17-32;